

DrFER: Learning Disentangled Representations for 3D Facial Expression Recognition

Hebeizi Li¹, Hongyu Yang^{2,3}, Di Huang¹

¹ School of Computer Science and Engineering, Beihang University, Beijing, China

² Institute of Artificial Intelligence, Beihang University, Beijing, China

³ Shanghai Artificial Intelligence Laboratory, Shanghai, China

Abstract—Facial Expression Recognition (FER) has consistently been a focal point in the field of facial analysis. In the context of existing methodologies for 3D FER or 2D+3D FER, the extraction of expression features often gets entangled with identity information, compromising the distinctiveness of these features. To tackle this challenge, we introduce the innovative DrFER method, which brings the concept of disentangled representation learning to the field of 3D FER. DrFER employs a dual-branch framework to effectively disentangle expression information from identity information. Diverging from prior disentanglement endeavors in the 3D facial domain, we have carefully reconfigured both the loss functions and network structure to make the overall framework adaptable to point cloud data. This adaptation enhances the capability of the framework in recognizing facial expressions, even in cases involving varying head poses. Extensive evaluations conducted on the BU-3DFE and Bosphorus datasets substantiate that DrFER surpasses the performance of other 3D FER methods.

I. INTRODUCTION

Facial Expression Recognition (FER) represents a crucial research area within the domain of facial analysis, playing a pivotal role in elucidating human emotions, cognitive processes, and behavioral patterns. FER techniques find applications in various real-world contexts, such as psychological analysis, human-computer interaction, and traffic safety, thereby underscoring its significance in both scientific research and practical applications.

The advancements in computer vision and image processing technologies have led to significant developments in FER. The origin can be traced back to the 1970s, when Ekman and Friesen [5] identified and defined six fundamental human facial expressions, including anger, disgust, fear, happiness, sadness, and surprise. Early FER approaches are mainly performed on 2D data, including static images [31][12] and dynamic videos [18][43], where both manual operator-based methods and machine learning solutions, such as deep neural networks, have been actively employed. However, 2D FER suffers from several intrinsic issues, *i.e.*, illumination and viewpoint variations, making its robustness problematic in the scenarios with high reliability requirements.

With the advent of 3D data scanning equipment and rapid advancement of 3D modeling techniques, expression recognition using 3D data has emerged as a new trend in face analysis, enabling more thorough analysis of subtle facial movements. Moreover, since shape data are reputed to be insensitive to varying lighting and convenient for pose correction, it allows for the solutions of many issues that cannot be addressed in 2D FER. In recent years, 3D FER methods have evolved into three main categories: model-based, feature-based, and deep learning-based approaches, which aim to enhance the representation of expression information from various perspectives, capitalizing on the advan-

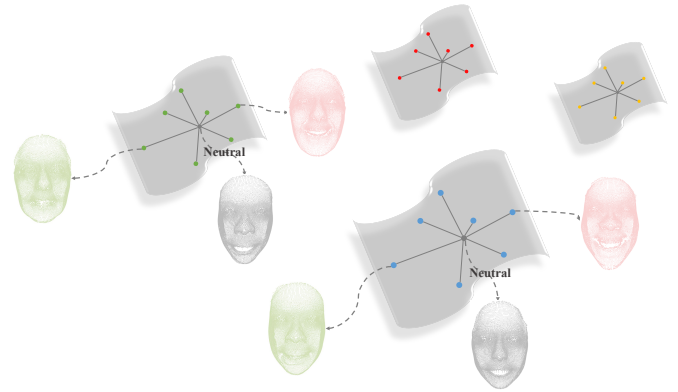


Fig. 1. Illustrations of 3D facial shape space. Human expressions occupy manifolds within a high-dimensional space, which exhibit similar patterns across different individuals and the center of each expression manifold corresponds to the neutral expression.

tages of 3D shape data. Furthermore, there has been a rise in multi-modal FER methods that combine different clues from both 2D texture information and 3D geometry information for expression analysis. While significant progress has been made in these areas, there are still shortcomings in existing 3D FER and 2D+3D FER studies. Many of these methods primarily focus on enhancing the expressiveness of features related to geometric information or addressing domain gaps for multi-modal feature fusion. Unfortunately, they often mix expression features with identity information, resulting in a loss of distinctiveness in these features.

Prior facial expression analysis [2] has posited that the latent variables representing identity and expression exist on a manifold within a high-dimensional space. As depicted in Figure 1, the expression manifolds exhibit similarities across individuals, highlighting the goal of FER methods to learn a universal expression representation. Furthermore, Grasshof *et al.* [8][9] have observed that apathy (the neutral expression in the datasets) serves as the central point for all expressions, implying that the trajectories leading to various expressions, achieved by adjusting expression intensity, all originate from this neutral point. This discovery suggests an implicit connection between different emotional faces with the same identity, centered around the neutral face. These findings provide two key inspirations for subsequent research. First, a universal expression representation can be constructed by learning the transformations from expressive to neutral faces. Second, the identity information can be extracted by learning the neutral expressions of different individuals. While such disentanglement concept has found successful applications in numerous 2D FER solutions [14][1][23] and has been effectively utilized in 3D face reconstruction tasks [26][15],

its integration into the 3D FER domain represents a novel development as of now.

In this study, we present a novel method named DrFER, which leverages the observations above to disentangle facial expression representations from identity-related factors for 3D FER. In particular, unlike prior 3D disentanglement methods that primarily use mesh as source data, a key distinction of our approach is the use of facial point cloud data as input, chosen for its inherent robustness to variations in facial pose. To accommodate this choice, we have made substantial adaptations to both the configuration of the loss functions and the network architecture. Specifically, to address the challenge that the features extracted from point clouds do not conform to the standard distribution, we choose not to use KL Loss and JS Loss, which are commonly employed as disentanglement supervisions. Instead, we carefully design the loss functions to regulate the latent space. Additionally, the network architecture, based on PointNet++ [28], is thoughtfully designed to achieve effective disentanglement and re-coupling. These adaptations enable the effective application of the disentanglement framework to point cloud data, enhancing its robustness and performance in 3D FER. The contributions of this study can be briefly summarized as follows:

- This paper introduces an innovative approach, DrFER, which marks the first application of the disentanglement paradigm within the field of 3D FER.
- The framework represents a notable advancement over prior endeavors, primarily through the loss functions and network architecture adeptly designed for the analysis of 3D point cloud data.
- The proposed approach achieves a state-of-the-art level of performance on both the BU-3DFE and Bosphorus datasets, positioning it alongside the outcomes achieved by other 2D+3D FER techniques. Importantly, DrFER demonstrates robustness in handling rotational poses.

II. RELATED WORK

A. 3D Facial Expression Recognition

Wang *et al.* [39] in their pioneering work laid the foundation for utilizing 3D data in facial expression recognition. Subsequently, a number of methods have been developed with a focus on extracting 3D facial geometric features for FER and they can be broadly categorized into two major types: model-based [24][7] and feature-based [41][34][44]. Model-based methods typically derive expression information by modeling generalized shape statistics and fitting 3D facial expression samples to retrieve the corresponding fitting coefficients. For instance, Mpiperis *et al.* [24] introduced a bilinear elastically deformable model capable of estimating both identity and expression parameters, with the latter being utilized for expression recognition. Gong *et al.* [7] partitioned the 3D face into a Base Face Shape Component and an Expression Shape Component, where the expression-related component was employed to extract expression features. On the other hand, feature-based approaches applied various feature operators on 3D scans or computed corresponding 2D shape attribute maps. These numerical features are then utilized by a classifier to predict the FER results. For example, Yang *et al.* [41] computed scattering features on depth, normal, and shape index maps and used SVM for expression

classification. However, the FER accuracy of these methods heavily rely on the design of these operators or hand-crafted features.

With the rapid advancements in deep learning technology, its applications have extended into the field of 3D facial expression recognition. Notably, Chen *et al.* [3] presented an innovative model known as the Fast and Light Manifold CNN (FLM-CNN). Their approach involved a modification of the weighting mechanism, inspired by human vision, resulting in the development of a highly precise and rotation-invariant model for FER. While there exist numerous deep learning methods that leverage 2D+3D multimodal data, the wealth of geometric information inherent in pure 3D data remains an unexplored frontier with significant potential for further investigation.

B. Multi-modal Facial Expression Recognition

To combine 2D texture information and 3D geometric information, several studies have incorporated 2D and 3D multi-modal data to enhance the accuracy of FER. In particular, Li *et al.* [20] combined local texture descriptors and shape operators with multistage gradients, employing SVM for training and classification. In another work, Li *et al.* [21] pioneered the use of Convolutional Neural Networks (CNN) in 2D + 3D FER. Their proposed DF-CNN extracted features from various sources, including texture maps, depth maps, normal vector maps, and shape index maps, which were then stacked and fed into the network for expression classification. Zhu *et al.* [46] introduced a DA-CNN model incorporating an attention mechanism to enhance classification ability of the network, while Jiao *et al.* [17] presented FA-CNN, which leveraged attention mechanism to identify discriminative facial regions within multi-modal data. Besides, Lin *et al.* [22] proposed OGF²Net, which employed orthogonal loss to guide the fusion of multi-modal features. Sui *et al.* conducted a series of studies [33][32] where they utilized facial landmarks as priors for generating masks, strengthening the capacity to extract features. In their latest work [48], they improved the mask to a curvature-aware soft mask and integrated a multi-modal attention fusion module, achieving state-of-the-art performance.

In current multi-modal FER methods, the workflow typically includes utilizing distinct networks to extract features from 2D and 3D data, followed by feature fusion through an additional module. However, the existing research has primarily emphasized improving representation within each modality and fusing features across modalities, without explicitly separating the identity information mixed in the extracted expression features.

C. Disentangled Face Representations

Recently, there has been a growing interest in applying disentanglement techniques to face-related applications, including age-invariant face recognition [38][11], face editing [36][45][4], and face reenactment [10]. Particularly, in the 3D domain, a number of studies have delved into 3D face reconstruction [26][15] with a focus on achieving precise results through the disentanglement of expression and identity variables. These investigations underscore the effectiveness of the disentanglement concept in the field of 3D face analysis.

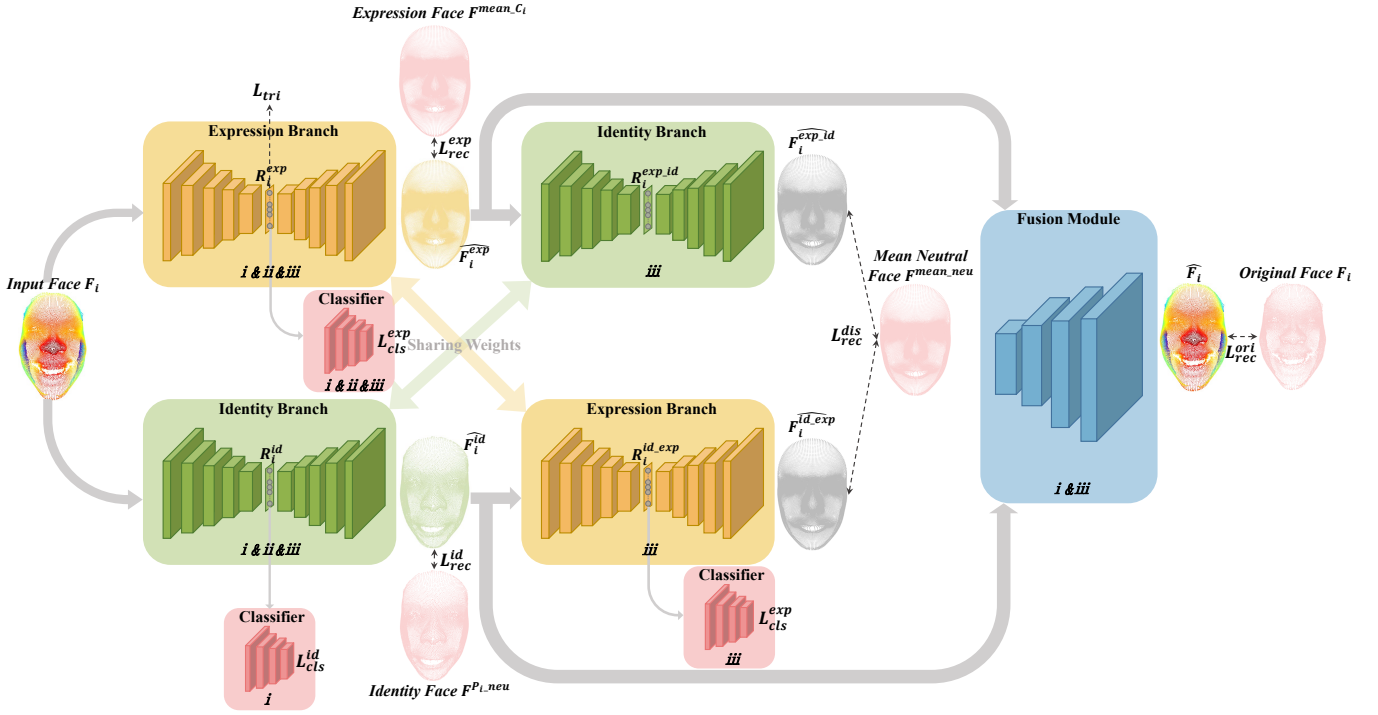


Fig. 2. Method overview. The proposed DrFER model comprises two key components: the disentangling component and the fusion component. The former employs a dual-branch architecture to explicitly learn expression and identity features, and generate the corresponding de-identity and de-expression faces, respectively. The model subsequently recombines these disentangled faces in a cross-over manner and reconstruct the original face with the fusion component, facilitating the disentanglement process. To guide the training process effectively, a series of training losses are employed, including those specifically tailored for point cloud data. The training stages corresponding to each module are labeled with lowercase Roman numerals in the figure.

Furthermore, there are several studies exploring FER via disentangled representation learning [14][1][23]. For instance, Jiang *et al.* [14] proposed a method that decomposes pose, identity, and expression information in the embedding space, leading to improved FER accuracy. Chang *et al.* [1] augmented their disentangled network with optical flow information and enforced constraints on the reconstruction results through cycle consistency loss. Liu *et al.* [23] adopted a metric learning approach to extract expression information by comparing original expression images with the generated neutral face images. These studies convincingly demonstrated the potential benefits of disentanglement techniques in enhancing expression recognition accuracy. To the best of our knowledge, this paper represents the pioneering effort to introduce a disentangled representation learning approach specifically designed for 3D FER.

III. METHOD

This section provides a detailed description of the proposed method. We outline the framework, network architecture, training strategy, and loss function used.

A. Overview

The proposed disentanglement approach comprises two key components, *i.e.*, the disentangling component and the fusion component, as illustrated in Figure 2. Given that diverse expressions originate from a neutral face of an individual, the disentangling component of DrFER thus employs a dual-branch network with two identical encoders to explicitly learn expression and identity features, respectively. The model follows the general disentanglement paradigm, intertwining the produced de-identity and de-expression faces in a cross-over fashion and re-generate 3D faces with

the fusion component. These operations not only facilitate the disentanglement learning process but also ensure the comprehensive capture of essential information. To guide the training process towards enhanced accuracy, a range of training losses is employed, including the customized Chamfer distance metric and triplet loss tailored for 3D point cloud data. Upon model convergence, the extracted expression feature is fed into a classification head to make the final decision.

B. Network Architecture

Formally, the input 3D face point cloud is represented as $F_i \in \mathbb{R}^{n \times 3}$ ($i \in [1, \dots, m]$), where n represents the number of points, and m is the count of input 3D face scans. Since the model operates under the assumption that expressions and identities inhabit distinct and mutually independent feature spaces, two dedicated branches, Φ_{exp} and Φ_{id} , are employed to handle expression and identity information in F_i , respectively. Both branches share an identical *Encoder-Decoder* structure as illustrated in Figure 3 (a), which is implemented based on Pointnet++ [28]. The encoder contains three *set abstraction* levels, and each is made of three key layers: *Sampling layer*, *Grouping layer* and *Pointnet layer*. The *Sampling layer* selects a set of centroid points from the input points, *Grouping layer* searches for neighboring points of the centroids, and *Pointnet layer* encodes the local region patterns into feature vectors. The decoder encompasses multiple fully-connected layers that decode the high-dimensional latent features into a 3D face point cloud. To summarize, the two branches produce latent representations, namely R_i^{exp} and $R_i^{id} \in \mathbb{R}^{n \times d}$ (with d representing the dimension) in the feature space, as well as the corresponding faces F_i^{exp} and F_i^{id} in the

observation space. Notably, the expression feature is denoted as residing in a 1024-dimensional space.

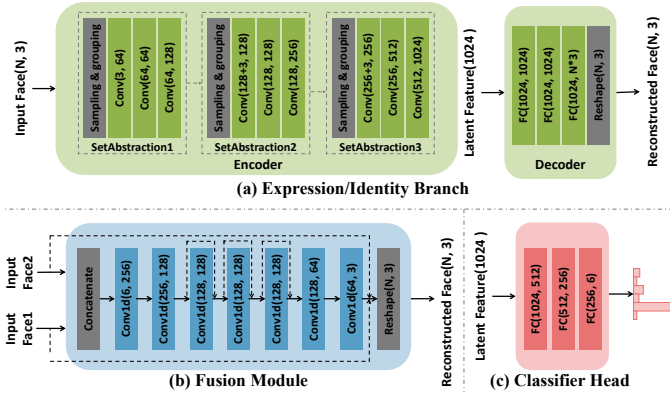


Fig. 3. Detailed architectures of the proposed expression/identity branch, the cross-modal fusion module, and the classifier.

To ensure that the two branches learn independent information, they are interconnected in a cross-over manner, leading to the derivation of new latent representations $R_i^{exp,id}$ and $R_i^{id,exp}$, along with newly reconstructed faces $F_i^{exp,id}$ and $F_i^{id,exp}$. For instance, in the upper stream of Figure 2, input F_i is fed into the expression branch Φ_{exp} to yield a face $F_i^{\hat{exp}}$ containing only the original expression information. Subsequently, $F_i^{\hat{exp}}$ is passed through the identity branch Φ_{id} to generate a face $F_i^{exp,id}$ devoid of both expression and identity information. Ideally, after the operations above, the representations of both streams do not retain information specific to the given input face and the mean neutral face $F^{mean,neu}$ should be precisely reconstructed. Notably, no supplementary modules are introduced during the cross-connection process, it is achieved by sharing weights with the original dual-branch architecture, thereby facilitating their concurrent optimization.

Moreover, the outputs of the two original disentanglement branches can be fused through a fusion module, denoted as Υ , to reconstruct the original input face, represented as \hat{F}_i . The architecture of this fusion module is depicted in Figure 3 (b), which can generate a face corresponding to the expression information from $Face_1$ and the identity property from $Face_2$. The primary objective of the fusion module is to assimilate the two input face point clouds by harmonizing their respective feature components, ultimately reconstructing a comprehensive facial representation. When the face pair consists of faces $F_i^{\hat{exp}}$ and $F_i^{\hat{id}}$, F_i should accurately be reconstructed. In particular, to strike a balance between the high-level semantic information and the observed point cloud information, skip connections have been incorporated at multiple scales within the fully connected layers of the fusion module. This strategic inclusion ensures that the module captures an ample amount of information during feature extraction.

Given that our primary objective is facial expression recognition utilizing the expression feature R_i^{exp} , we include an auxiliary classifier within the expression branch to oversee and guide the learning process. The architecture of this classifier is depicted in Figure 3 (c).

C. Training Strategy & Loss Functions

We apply a multi-stage strategy to stabilize the training process of the whole network, including the following steps:

- i. Pretrain the encoders of Φ_{exp} and Φ_{id} with two specific classifiers and pretrain the fusion module Υ with the ground-truth face scans as supervision.
- ii. Fine-tune the two branches Φ_{exp} and Φ_{id} individually using the reconstruction constraints.
- iii. Perform end-to-end training with a very small learning rate after joining the cross-over setup and the fusion module Υ .

To be specific, considering that pre-training in categorization is the most direct way for the encoders to learn discriminative features, we introduce the expression and identity recognition tasks to pre-train the encoders in the first phase. Let ϵ_{exp} and ϵ_{id} be the auxiliary classifiers for the expression and identity branches, respectively, the loss terms are defined as:

$$L_{stagei}^{exp} = L_{cls}^{exp} = \ell_{CE}(\epsilon_{exp}(R_i^{exp}), C_i), \quad (1)$$

$$L_{stagei}^{id} = L_{cls}^{id} = \ell_{CE}(\epsilon_{id}(R_i^{id}), P_i), \quad (2)$$

where ℓ_{CE} denotes the cross-entropy loss and C_i and P_i indicate the corresponding ground-truth labels of the sample F_i . Furthermore, the fusion module Υ rebuilds the original face using expression-identity face pairs. In particular, we group the faces by labels C_i , P_i and calculate the mean faces F^{mean,C_i} and $F^{P_i,neu}$. The pair $(F^{mean,C_i}, F^{P_i,neu})$ is used as the input to the fusion module to reconstruct F_i . The reconstruction loss is formulated as:

$$L_{stagei}^{fusion} = L_{rec}^{ori} = d_{CD}(\hat{F}_i, F_i), \quad (3)$$

where d_{CD} represents the chamfer distance [6] between two point clouds.

In the second stage, we leverage the reconstruction task to fine-tune the encoders and train their respective decoders. This strategy aligns with insights from previous studies [8], [9], which posit that the neutral face of an individual serves as the central point within the corresponding high-dimensional expression space. This neutral face can be regarded as predominantly containing identity information, thus making it a suitable representation of identity alone. Conversely, from a statistical analysis perspective, the average face corresponding to a specific expression type is assumed to lack identity information and predominantly encapsulate expression-related details. Hence, we utilize F^{mean,C_i} and $F^{P_i,neu}$ as ground-truth representations for the disentanglement of these two kinds of information through a reconstruction task. This training loss can be defined as follows:

$$L_{rec}^{exp} = d_{CD}(F_i^{\hat{exp}}, F^{mean,C_i}), \quad (4)$$

$$L_{rec}^{id} = d_{CD}(F_i^{\hat{id}}, F^{P_i,neu}). \quad (5)$$

To further constrain the feature space learned by the expression branch, we exploit a triplet loss [30] which brings samples of the same class closer together and samples of different classes farther apart. This triplet loss is represented as:

$$L_{tri} = \max\left(\|R_A - R_P\|^2 - \|R_A - R_N\|^2 + \alpha, 0\right), \quad (6)$$

where R_A is the feature of an anchor sample A , R_P and R_N denotes the features of the positive and negative samples, respectively, and α is a hyper-parameter to bound the distance between the positive and negative classes. It is important to highlight that our approach employs the triplet loss and classification loss instead of the commonly used KL divergence loss in prior 3D disentanglement frameworks designed for mesh data as input. The reason behind this choice lies in the fact that, unlike the explicit expression and identity variables present in 3D Morphable Models (3DMM), it is not straightforward to apply Gaussian distribution regularity ($N(0,1)$) to the expression features extracted from the point cloud data. This consideration motivates the adoption of the triplet loss, a commonly used metric in face recognition, to effectively disentangle the features. Overall, the losses in the second stage include:

$$L_{stageii}^{exp} = L_{rec}^{exp} + L_{tri} + L_{cls}^{exp}, \quad (7)$$

$$L_{stageii}^{id} = L_{rec}^{id}. \quad (8)$$

In the third stage, we further impose constraints on the outcomes of the cross-over and fusion reconstructions. In cases where the cross-over structure is utilized, both the upper and lower streams are compared against the ground-truth $F^{mean.neu}$. To assess the accuracy of reconstruction, we employ the Chamfer distance, which was introduced in the second stage, and denote it as:

$$L_{rec}^{dis} = d_{CD}(F_i^{\hat{exp}.id}, F^{mean.neu}) + d_{CD}(F_i^{\hat{id}.exp}, F^{mean.neu}). \quad (9)$$

Besides, the reconstruction loss of the fusion module is consistent with (3). In summary, the comprehensive loss function employed in the third stage of the end-to-end training is formulated as:

$$L_{stageiii} = \underbrace{L_{cls}^{exp} + L_{tri} + L_{rec}^{exp}}_{\Phi_{exp}} + \underbrace{L_{rec}^{id}}_{\Phi_{id}} + \underbrace{L_{rec}^{dis}}_{\Phi_{exp}, \Phi_{id}} + \underbrace{\lambda L_{rec}^{ori}}_{\Phi_{exp}, \Phi_{id}, \gamma}, \quad (10)$$

where λ is a hyper-parameter used for balancing the training critics. The various network modules that are supervised by the losses are labeled below the equation.

IV. EXPERIMENTS

In this section, we present the results of the proposed DrFER model on the publicly available BU-3DFE and Bosphorus datasets. We aim to validate the effectiveness of our method through a comparison with other state-of-the-art approaches and extensive ablation studies. The following sections provide details on the datasets used, implementation details, experimental results, and visualizations of the outcomes.

A. Datasets

BU-3DFE [42]: BU-3DFE is the most commonly used publicly available dataset for academic research on 3D FER, which contains 2,500 scans of 100 subjects between the ages of 18 and 70 (56 females and 44 males). Each subject has 25 samples of seven expressions in total: one neutral sample and six basic expressions samples of four different intensities. We follow a consistent experimental protocol with previous work [3][48][32][22] for fair comparisons. In this protocol, we randomly select 60 subjects out of total 100 subjects and fix them during the entire experiment. 10-fold cross-validation

experiments are conducted on the sub-dataset which consists of six expressions of the two highest intensities from these 60 subjects. The cross-validation groups the 60 subjects into 10 subsets, each of which is selected once as the test set and the remaining 9 subsets are used as the training set. This validation process is repeated for 100 times to minimize jitters in the experimental results.

Bosphorus [29]: Bosphorus comprises a total of 4,666 3D face scans collected from 105 subjects within the age range of 25 to 35. Among these subjects, 65 individuals exhibit the complete set of six basic expressions, each with a single intensity level. For our experimental setup, we opt to utilize a subset of 60 subjects from this group, following the 10-fold cross-validation protocol, which is aligned with the approach used in the BU-3DFE dataset.

B. Implementation Details

Regarding data preprocessing, we perform rigid registration on all point clouds, aligning them to a common 3D mesh. Following this, we resample the point clouds to a uniform size of 39,923 points. For each face scan, we choose 2,048 points as input for the network, in line with the farthest point sampling technique as employed in PointNet++ [28]. Furthermore, we augment the dataset by introducing random dropout and random scale transformations during each training epoch.

The network is trained using the Adam optimizer with beta values (0.9, 0.999). In Stage i, the initial learning rate is set to 0.001, and both branches and the fusion module are trained with a batch size of 24. In Stage ii, the learning rate is adjusted to 0.0001 for fine-tuning the two branches with the reconstruction tasks. In Stage iii, to mitigate the risk of overfitting, the learning rate is further reduced to 0.00001, and fine-tuning is performed on the entire network. During the fine-tuning phase, the cross-over structure is introduced, necessitating an adaptation of the batch size to 16. The hyperparameters in (6) and (10) are set to $\alpha = 0.3$ and $\lambda = 0.1$. Training is carried out within the PyTorch framework, and the model is validated using an NVIDIA GeForce RTX 3080 Ti GPU.

C. Quantitative comparison

1) Results on BU-3DFE: TABLE I provides a comparison of our approach against state-of-the-art methods achieved on the BU-3DFE dataset, where the baseline counterpart entails the direct utilization of the expression branch trained in stage i, amalgamated with the classifier head for expression recognition. Remarkably, our method achieves an accuracy of 89.15%, surpassing other 3D-based approaches that utilize either hand-crafted or deep learning features. Furthermore, our method, which exclusively employs 3D data, closely approaches the performance achieved by 2D+3D multi-modal methods. To ensure an equitable evaluation, we also consider the results reported by these approaches when exclusively utilizing 3D data. The comparative findings unequivocally establish our method as the top performer in the 3D data-only scenario.

2) Results on Bosphorus: TABLE II presents the comparative results on the Bosphorus dataset. In a similar fashion, our approach notably surpasses other methodologies that exclusively rely on 3D data, underscoring its superior performance. It is worth noting that while the work by Jiao

TABLE I

QUANTITATIVE COMPARISON ON BU-3DFE. †INDICATES THAT THE RESULTS ACHIEVED BY USING ONLY 3D MODALITY ARE ALSO REPORTED.

Method	Modality	Feature	Accuracy(%)
Li <i>et al.</i> [20]	2D+3D	Hand-crafted	86.32
Li <i>et al.</i> [21]	2D+3D	Deep Learning	86.86
Wei <i>et al.</i> †[40]	2D+3D	Deep Learning	88.03
Zhu <i>et al.</i> †[46]	2D+3D	Deep Learning	88.35
Jan <i>et al.</i> †[13]	2D+3D	Deep Learning	88.54
Zhu <i>et al.</i> †[47]	2D+3D	Deep Learning	88.75
Ni <i>et al.</i> †[25]	2D+3D	Deep Learning	88.91
Lin <i>et al.</i> †[22]	2D+3D	Deep Learning	89.05
Jiao <i>et al.</i> [17]	2D+3D	Deep Learning	89.11
Oyebade <i>et al.</i> †[27]	2D+3D	Deep Learning	89.31
Jiao <i>et al.</i> [16]	2D+3D	Deep Learning	89.72
Sui <i>et al.</i> †[33]	2D+3D	Deep Learning	89.82
Sui <i>et al.</i> †[32]	2D+3D	Deep Learning	90.08
Zhu <i>et al.</i> †[48]	2D+3D	Deep Learning	90.24
Wei <i>et al.</i> [40]	3D	Deep Learning	74.44
Tang <i>et al.</i> [34]	3D	Hand-crafted	74.51
Gong <i>et al.</i> [7]	3D	Hand-crafted	76.22
Ni <i>et al.</i> [25]	3D	Deep Learning	80.11
Li <i>et al.</i> [19]	3D	Hand-crafted	80.14
Jan <i>et al.</i> [13]	3D	Deep Learning	81.83
Zhu <i>et al.</i> [48]	3D	Deep Learning	84.03
Zhen <i>et al.</i> [44]	3D	Hand-crafted	84.50
Oyebade <i>et al.</i> [27]	3D	Deep Learning	84.72
Yang <i>et al.</i> [41]	3D	Hand-crafted	84.80
Lin <i>et al.</i> [22]	3D	Deep Learning	85.20
Chen <i>et al.</i> [3]	3D	Deep Learning	86.67
Sui <i>et al.</i> [32]	3D	Deep Learning	86.97
Zhu <i>et al.</i> [47]	3D	Deep Learning	87.19
Sui <i>et al.</i> [33]	3D	Deep Learning	87.28
Zhu <i>et al.</i> [46]	3D	Deep Learning	87.69
Ours (Baseline)	3D	Deep Learning	84.83
Ours	3D	Deep Learning	89.15 (†4.32)

et al. [16] merely provides experimental results employing multi-modal data, our method outperforms their approach by a large margin of 3.14% on the Bosphorus dataset.

3) *Comparison with the Baseline:* It is remarkable that our method demonstrates significant improvements of 4.32% and 3.54% when compared to the baseline models on the BU-3DFE and Bosphorus datasets, respectively. These results clearly illustrate that disentangled learning significantly improves the performance of our approach.

D. Ablation Studies

To further prove the validity of every component of our method, we conduct extensive ablation experiments on BU-3DFE, and the results are shown in TABLE III.

Evaluation of the loss functions. In the latter two training stages, we employ the cross-entropy loss (2) and the triplet loss (6) to constrain the learning of the expression feature space. We remove these two parts separately for comparison and find that the classification accuracy decreases, pointing to the value of these two kinds of losses for the overall supervision. Furthermore, drawing from prior research in the domain of disentanglement-based 3D face reconstruction [26][15], we attempt to employ Kullback-Leibler (KL) divergence loss and Jensen-Shannon (JS) divergence loss as constraints to govern the feature space distribution. However, these endeavors do not yield favorable outcomes. The experiments suggest that the features extracted from the given point cloud data do not conform to the standard distribution of 3DMM, leading us to abstain from the utilization of KL loss and JS loss in our final framework configuration.

TABLE II

QUANTITATIVE COMPARISON ON BOSPHORUS. †INDICATES THAT THE RESULTS ACHIEVED BY USING ONLY 3D MODALITY ARE ALSO REPORTED.

Method	Modality	Feature	Accuracy(%)
Tian <i>et al.</i> [35]	2D+3D	Deep Learning	79.17
Li <i>et al.</i> [20]	2D+3D	Hand-crafted	79.72
Li <i>et al.</i> [21]	2D+3D	Deep Learning	80.28
Wei <i>et al.</i> †[40]	2D+3D	Deep Learning	82.50
Jiao <i>et al.</i> [16]	2D+3D	Deep Learning	83.63
Ni <i>et al.</i> †[25]	2D+3D	Deep Learning	85.16
Sui <i>et al.</i> †[33]	2D+3D	Deep Learning	87.65
Sui <i>et al.</i> †[32]	2D+3D	Deep Learning	88.31
Lin <i>et al.</i> †[22]	2D+3D	Deep Learning	89.28
Zhu <i>et al.</i> †[48]	2D+3D	Deep Learning	89.36
Wei <i>et al.</i> [40]	3D	Deep Learning	65.00
Li <i>et al.</i> [19]	3D	Hand-crafted	75.83
Yang <i>et al.</i> [41]	3D	Hand-crafted	77.50
Ni <i>et al.</i> [25]	3D	Deep Learning	77.82
Zhu <i>et al.</i> [48]	3D	Deep Learning	81.25
Sui <i>et al.</i> [32]	3D	Deep Learning	82.06
Sui <i>et al.</i> [33]	3D	Deep Learning	82.86
Lin <i>et al.</i> [22]	3D	Deep Learning	83.55
Ours (Baseline)	3D	Deep Learning	83.23
Ours	3D	Deep Learning	86.77 (†3.54)

Evaluation of the network structure. We perform ablation experiments on the network structure to validate the design. Attention is given to the fusion module, which is a separate component in the whole framework. It is used to supervise the completeness of the features learned by the two branches and we ablate this module separately to justify the design. The experimental results reveal a reduction in classification accuracy upon its removal. The observation strongly indicates that the module plays a pivotal role in effectively encouraging the expression branch to acquire a more comprehensive understanding of expression-related information. Further, we ablate the skip connection setting in the fusion module. The result shows that the fusion module lacking skip connections exhibits an improvement in performance compared to the baseline. Nevertheless, the degree of improvement is relatively lower compared to the fusion module incorporating skip connections. This observation implies that the inclusion of skip connections enables the integration of multi-scale information, thereby facilitating the fusion reconstruction task and ultimately enhancing the overall expression recognition capability of the framework.

Evaluation of the training strategy. We employ a multi-stage training strategy that allows the framework to learn disentangled expression feature space step by step. We test the classification accuracy of the features extracted by the expression branch at the end of each training phase and report the results. The incremental enhancements in classification accuracy achieved through the fine-tuning process serve as compelling evidence that each stage of our fine-tuning is effective and supports the rationale behind employing a multi-stage training strategy.

E. Robustness to Rotation

Our method exhibits robustness to facial pose changes, which can be attributed to the utilization of 3D mode data. To further validate this aspect, we conducted additional experiments on the rotated data. Given that the BU-3DFE dataset only consists of frontal faces, we artificially introduce variations by rotating the samples and subsequently removing invisible points to simulate self-occlusion.

TABLE III

ABLATION EXPERIMENTS OF THE LOSS FUNCTIONS, THE FUSION MODULE, AND THE TRAINING STRATEGY.

Loss Function				Network Structure		Training Strategy			Accuracy
w/o L_{Tri}	w/o L_{cls}	w/ L_{KL}	w/ L_{JS}	w/o Fusion	w/o Skip Connection	Stage i	Stage ii	Stage iii	
✓						✓	✓	✓	85.92
	✓					✓	✓	✓	87.59
		✓				✓	✓	✓	85.98
			✓			✓	✓	✓	85.04
				✓		✓	✓	✓	87.15
					✓	✓	✓	✓	87.76
						✓			84.83
						✓	✓		86.67
						✓	✓	✓	89.15

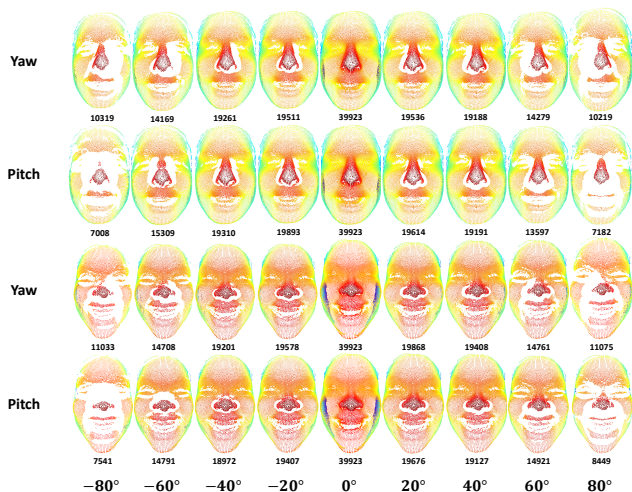


Fig. 4. Visualization of the rotated faces. The faces in the top two rows and the bottom two rows are from two different randomly selected subjects. Columns indicate different rotation angles. Faces in the same column have the same rotation angle. The numbers below each facial scan represent the points that are preserved after point cloud rotation.

We follow the general experimental protocol on BU-3DFE and randomly select 60 subjects for a 10-fold cross-over experiment. For each chosen subject, we rotate its 12 3D facial scans (six expressions, two highest intensities) to generate new data. We ultimately pick 16 rotations (pitch and yaw: $-80^\circ, -60^\circ, -40^\circ, -20^\circ, 20^\circ, 40^\circ, 60^\circ, 80^\circ$) and randomly select two samples for the presentation of rotated data as Figure 4 shows. As the rotation angle increases, the number of the occluded points increases and at the extreme angle ($\pm 80^\circ$), significantly fewer points are remained in the pitch angle transformation than in the yaw angle transformation.

Figure 5 sequentially illustrates the recognition results for the 17 poses (plus 0°) that we test. Given that both the disentangled method and the baseline method utilize point cloud data as input, it is evident that their results demonstrate certain similarities. However, through a comprehensive evaluation, it becomes apparent that the disentangled approach exhibits a notable superiority over the baseline. With increasing rotation angles, our recognition accuracy decreases, but all of them is maintained at a high level (above 80%), which confirms the rotation-invariant capability of our method. We also notice that the variation of yaw angle has a smaller impact on the recognition accuracy, which we analyze to the fact that the left and right faces have some symmetry, and the network automatically focuses on the unoccluded other side in case of occluding one side. In

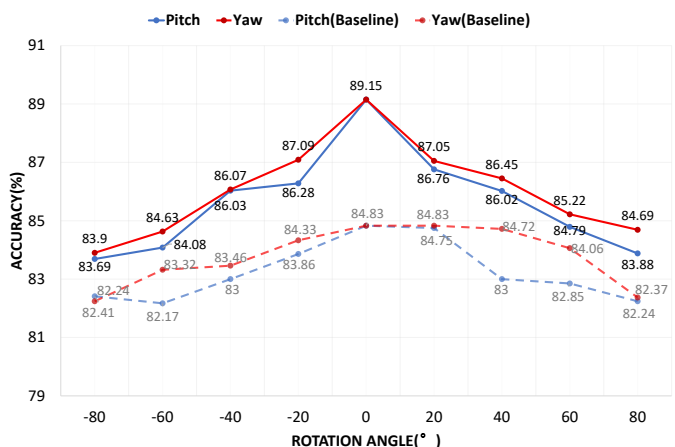


Fig. 5. Comparative results of the rotation experiment between the disentangled and the baseline methods. The results of these two methods are plotted as solid and dashed lines, where blue and red colors represent the pitch and yaw rotations, respectively.

general, the results of the rotation experiment suggest that our method has promising potential for handling 3D FER in more practical scenarios.

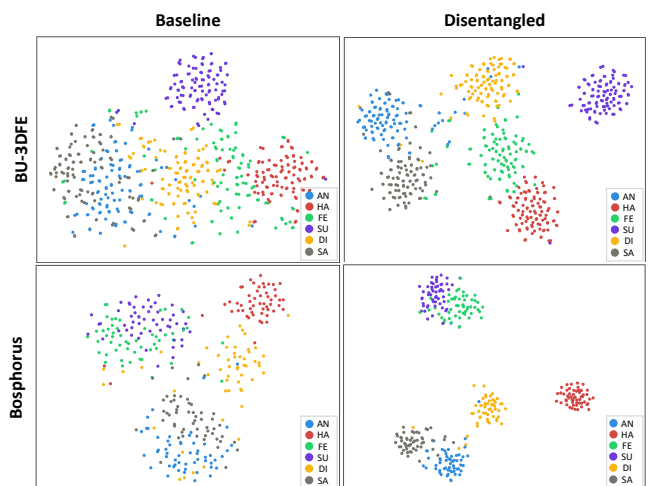


Fig. 6. T-SNE visualization of the expression features extracted by the baseline method and the proposed one on BU-3DFE and Bosphorus datasets. Six basic expressions are marked with different colors.

F. Visualization

To exemplify the efficacy of our disentanglement method, we employ t-SNE [37] to visualize the expression features extracted by both the baseline and our proposed method. In Figure 6, the first and second rows correspond to the BU-

3DFE and Bosphorus datasets, respectively. The left column represents the features before disentanglement, while the right column illustrates the features after disentanglement. It is readily apparent that the features extracted by the baseline method exhibit a lack of differentiation, characterized by fuzzy boundaries between expression categories. In contrast, our method yields features with dense clustering, demarcating clear and distinct boundaries for each expression category. These visualizations serve as compelling evidence that the disentangled expression features acquired through our approach are more amenable to classification tasks.

V. CONCLUSION

In this study, we introduce the concept of disentangled representation learning into 3D FER via our approach, Dr-FER. The method utilizes a dual-branch framework for 3D point cloud data, where the cross-over structure and fusion module enable concurrent learning of expression and identity information. Additionally, triplet loss and cross-entropy loss constrain the feature space for improved results on 3D point clouds. Experimental results demonstrate its superiority over other 3D FER methods, achieving comparable results to 2D+3D FER methods when using only 3D data. Dr-FER addresses 3D FER through disentangled representations learning, demonstrating robustness to pose variations and providing insights for future research in 3D and 2D+3D FER.

VI. ACKNOWLEDGMENTS

This work is partly supported by the National Key R&D Program of China (No. 2022ZD0161902), the National Natural Science Foundation of China (No. 62176012, 62202031), the Beijing Natural Science Foundation (No. 4222049), and the Fundamental Research Funds for the Central Universities.

REFERENCES

- [1] J.-R. Chang, Y.-S. Chen, and W.-C. Chiu. Learning facial representations from the cycle-consistency of face. In *ICCV*, 2021.
- [2] Y. Chang, C. Hu, R. Feris, and M. Turk. Manifold based analysis of facial expression. *IVC*, 2006.
- [3] Z. Chen, D. Huang, Y. Wang, and L. Chen. Fast and light manifold cnn based 3d facial expression recognition across pose variations. In *ACM MM*, 2018.
- [4] Y. Deng, J. Yang, D. Chen, F. Wen, and X. Tong. Disentangled and controllable face image generation via 3d imitative-contrastive learning. In *CVPR*, 2020.
- [5] P. Ekman and W. V. Friesen. Constants across cultures in the face and emotion. *J Pers Soc Psychol*, 1971.
- [6] H. Fan, H. Su, and L. J. Guibas. A point set generation network for 3d object reconstruction from a single image. In *CVPR*, 2017.
- [7] B. Gong, Y. Wang, J. Liu, and X. Tang. Automatic facial expression recognition on a single 3d face by exploring shape deformation. In *ACM MM*, 2009.
- [8] S. Grabhof, H. Ackermann, S. S. Brandt, and J. Ostermann. Apathy is the root of all expressions. In *FG*, 2017.
- [9] S. Grasshof, H. Ackermann, S. S. Brandt, and J. Ostermann. Multi-linear modelling of faces and expressions. *TPAMI*, 2020.
- [10] P.-H. Huang, F.-E. Yang, and Y.-C. F. Wang. Learning identity-invariant motion representations for cross-id face reenactment. In *CVPR*, 2020.
- [11] Z. Huang, J. Zhang, and H. Shan. When age-invariant face recognition meets face age synthesis: A multi-task learning framework. In *CVPR*, 2021.
- [12] T. Jabit, M. H. Kabir, and O. Chae. Local directional pattern (ldp) for face recognition. In *ICCE*, 2010.
- [13] A. Jan, H. Ding, H. Meng, L. Chen, and H. Li. Accurate facial parts localization and deep learning for 3d facial expression recognition. In *FG*, 2018.
- [14] J. Jiang and W. Deng. Disentangling identity and pose for facial expression recognition. *TAC*, 2022.
- [15] Z.-H. Jiang, Q. Wu, K. Chen, and J. Zhang. Disentangled representation learning for 3d face shape. In *CVPR*, 2019.
- [16] Y. Jiao, Y. Niu, T. D. Tran, and G. Shi. 2d+ 3d facial expression recognition via discriminative dynamic range enhancement and multi-scale learning. *arXiv:2011.08333*, 2020.
- [17] Y. Jiao, Y. Niu, Y. Zhang, F. Li, C. Zou, and G. Shi. Facial attention based convolutional neural network for 2d+ 3d facial expression recognition. In *VCIP*, 2019.
- [18] I. Kotsia and I. Pitas. Facial expression recognition in image sequences using geometric deformation features and support vector machines. *TIP*, 2006.
- [19] H. Li, L. Chen, D. Huang, Y. Wang, and J.-M. Morvan. 3d facial expression recognition via multiple kernel learning of multi-scale local normal patterns. In *ICPR*, 2012.
- [20] H. Li, H. Ding, D. Huang, Y. Wang, X. Zhao, J.-M. Morvan, and L. Chen. An efficient multimodal 2d+ 3d feature-based approach to automatic facial expression recognition. *CVIU*, 2015.
- [21] H. Li, J. Sun, Z. Xu, and L. Chen. Multimodal 2d+ 3d facial expression recognition with deep fusion convolutional neural network. *TMM*, 2017.
- [22] S. Lin, M. Bai, F. Liu, L. Shen, and Y. Zhou. Orthogonalization-guided feature fusion network for multimodal 2d+ 3d facial expression recognition. *TMM*, 2020.
- [23] X. Liu, B. V. Kumar, P. Jia, and J. You. Hard negative generation for identity-disentangled facial expression recognition. *PR*, 2019.
- [24] I. Mpipieris, S. Malassiotis, and M. G. Strintzis. Bilinear models for 3-d face and facial expression recognition. *TIFS*, 2008.
- [25] R. Ni, B. Yang, X. Zhou, A. Cangelosi, and X. Liu. Facial expression recognition through cross-modality attention fusion. *TCDS*, 2022.
- [26] N. Olivier, K. Baert, F. Danieau, F. Multon, and Q. Avril. Facetunegan: Face autoencoder for convolutional expression transfer using neural generative adversarial networks. *C&G*, 2023.
- [27] O. K. Oyedotun, G. Demisse, A. El Rahman Shabayek, D. Aouada, and B. Ottersten. Facial expression recognition via joint deep learning of rgb-depth map latent representations. In *ICCV workshops*, 2017.
- [28] C. R. Qi, L. Yi, H. Su, and L. J. Guibas. Pointnet++: Deep hierarchical feature learning on point sets in a metric space. *NeurIPS*, 2017.
- [29] A. Savran, N. Alyüz, H. Dibekliöglü, O. Çelikutan, B. Gökberk, B. Sankur, and L. Akarun. Bosphorus database for 3d face analysis. In *BIOID*, 2008.
- [30] F. Schroff, D. Kalenichenko, and J. Philbin. Facenet: A unified embedding for face recognition and clustering. In *CVPR*, 2015.
- [31] C. Shan, S. Gong, and P. W. Mcowan. Robust facial expression recognition using local binary patterns. In *ICIP*, 2005.
- [32] M. Sui, H. Li, Z. Zhu, and F. Zhao. Afnet-m: Adaptive fusion network with masks for 2d+ 3d facial expression recognition. In *ICIP*, 2023.
- [33] M. Sui, Z. Zhu, F. Zhao, and F. Wu. Ffnet-m: Feature fusion network with masks for multimodal facial expression recognition. In *ICME*, 2021.
- [34] H. Tang and T. S. Huang. 3d facial expression recognition based on properties of line segments connecting facial feature points. In *FG*, 2008.
- [35] K. Tian, L. Zeng, S. McGrath, Q. Yin, and W. Wang. 3d facial expression recognition using deep feature fusion cnn. In *ISSC*, 2019.
- [36] L. Tran, X. Yin, and X. Liu. Disentangled representation learning gan for pose-invariant face recognition. In *CVPR*, 2017.
- [37] L. Van der Maaten and G. Hinton. Visualizing data using t-sne. *JMLR*, 2008.
- [38] H. Wang, D. Gong, Z. Li, and W. Liu. Decorrelated adversarial learning for age-invariant face recognition. In *CVPR*, 2019.
- [39] J. Wang, L. Yin, X. Wei, and Y. Sun. 3d facial expression recognition based on primitive surface feature distribution. In *CVPR*, 2006.
- [40] X. Wei, H. Li, J. Sun, and L. Chen. Unsupervised domain adaptation with regularized optimal transport for multimodal 2d+ 3d facial expression recognition. In *FG*, 2018.
- [41] X. Yang, D. Huang, Y. Wang, and L. Chen. Automatic 3d facial expression recognition using geometric scattering representation. In *FG*, 2015.
- [42] L. Yin, X. Wei, Y. Sun, J. Wang, and M. J. Rosato. A 3d facial expression database for facial behavior research. In *FG*, 2006.
- [43] G. Zhao and M. Pietikainen. Dynamic texture recognition using local binary patterns with an application to facial expressions. *TPAMI*, 2007.
- [44] Q. Zhen, D. Huang, Y. Wang, and L. Chen. Muscular movement model-based automatic 3d/4d facial expression recognition. *TMM*, 2016.
- [45] Y. Zheng, Y.-K. Huang, R. Tao, Z. Shen, and M. Savvides. Unsupervised disentanglement of linear-encoded facial semantics. In *CVPR*, 2021.
- [46] K. Zhu, Z. Du, W. Li, D. Huang, Y. Wang, and L. Chen. Discriminative attention-based convolutional neural network for 3d facial expression recognition. In *FG*, 2019.
- [47] K. Zhu, Y. Wang, H. Yang, D. Huang, and L. Chen. Intensity enhancement via gan for multimodal facial expression recognition. In *ICIP*, 2020.
- [48] Z. Zhu, M. Sui, H. Li, and F. Zhao. Cmanet: Curvature-aware soft mask guided attention fusion network for 2d+ 3d facial expression recognition. In *ICME*, 2022.